JOURNAL OF GEOPHYSICAL RESEARCH, VOL. 98, NO. B4, PAGES 6623–6638, APRIL 10, 1993

Structure of Archean Crust and Passive Margin of Southwest Greenland From Seismic Wide-Angle Data

KARSTEN GOHL[1] AND SCOTT B. SMITHSON

Department of Geology and Geophysics, University of Wyoming, Laramie

To investigate the structure and composition of the Archean crust beneath the shelf of southwest Greenland parallel to the passive margin, we conducted an onshore/offshore seismic wide-angle experiment in 1989. One of our goals was to obtain a velocity/depth profile along the thinned continental or transitional crust to place constraints on the magmatic rifting history in the northern Labrador Sea. Seismic recording instruments at four locations along the coast recorded energy from an air gun array up to 400 km distance. Due to the dense shot spacing of 100 to 150 m we were able to identify continuous reflected and refracted phases from the upper to lower crust. Results from a one-dimensional extremal inversion indicated a high-velocity zone (HVZ) with P wave velocities of more than 7.2 km/s at the bottom of the transitional crust. Combined two-dimensional travel time forward modeling and inversion produced a velocity/depth model that contains midcrustal and lower crustal discontinuities between 12 and 25 km depth and a Moho dipping northward at 30 to 42 km depth. An average crustal velocity of about 6.6 km/s indicates a high portion of mafic components in the crust. The lowermost crust consists of a HVZ with a maximum thickness of 8 km and temperature-corrected velocities of 7.5 to 7.85 km/s. The HVZ may be explained by an underplated igneous complex often observed under passive margins worldwide. Metamorphism to garnet-pyroxene-granulite during postrift isobaric cooling of the 30- to 40-km-deep, thinned continental crust could explain the velocities that are higher than on other margins. A large volume of magmatic material must have been added to the crust but did not produce extrusions. Magmatic underplating of the thinned continental or transitional crust of SW Greenland is likely associated with a possible hot spot magmatism in the Davis Strait and Baffin Bay region. Magmatism associated with continental rifting was found to reach farther south along the northern and central part of the Archean block than previously thought.

INTRODUCTION

Rifting processes that lead to formation of new oceanic crust develop magmatism that may be intrusive and/or extrusive. Extrusive magmatism was very active during the opening of the Davis Strait and Baffin Bay but was lacking along the Labrador Sea margins during earlier stages of rifting. The Labrador Sea and Davis Strait basins separate the conjugate margins of oldest Archean crust in Greenland and Labrador (Figure 1). To study the effect of Cretaceous and early Tertiary magmatic rifting of an early Archean craton, a large-offset wide-angle and normal-incidence seismic experiment was conducted parallel to the southwest Greenland coast and along two fjords. The goal of the experiment was to obtain information on seismic velocities and structure along a transect from undisturbed continental crust into thinned continental or transitional oceanic-continental crust in the basin. The normal-incidence common midpoint (CMP) data do not contain many events and are currently being reprocessed. This paper analyzes the wide-angle seismic data obtained along the Greenland shelf. An analysis of a seismic transect from the shelf into the undisturbed Archean continental crust will appear in a later paper.

Combined onshore/offshore wide-angle data acquisitions in recent years have proven the advantage of large offset, densely spaced recordings [i.e., *GLIMPCE Seismic Refraction Working Group*, 1989; *Brocher and Moses*, 1990; *BABEL Working Group*, 1991]. The experimental design allows the integration of processing techniques from reflection seismology, such as deconvolution and coherency filtering, and forward/inverse modeling. To approximate an initial model for a two-dimensional (2-D) inversion, we derived localized one-dimensional (1-D) models using a tau-p inversion. 2-D travel time inversion and forward ray tracing were subsequently performed using the results from the 1-D velocity/depth model as initial values. Our modeling results provide new implications for the composition of the thinned continental crust close to the passive margin in SW Greenland with respect to the magmatic rifting history of the Labrador Sea and Davis Strait.

GEOLOGY AND PREVIOUS GEOPHYSICS

Our study area is located on the shelf and western edge of the Archean block of SW Greenland (Figure 2). The Archean block consists of several gneissic, granitic, and supracrustal complexes with ages between 2750 and 3800 Ma [*Bridgwater et al.*, 1976; *McGregor et al.*, 1986]. *Nutman et al.* [1989] suggest a juxtaposition of four Archean subterranes at about 2750 Ma, each terrane having evolved separately prior to juxtaposition. Profile WA and receiver stations UM, KA, IK are located along the Akia terrane. Station GR was placed on rocks of the Tasiusarsuaq terrane.

The Labrador Sea rifting event separated the Archean block of Greenland from its counterpart in Canada, the Nain Province [*Taylor*, 1972]. Rifting started in the southern Labrador Sea during the Late Cretaceous (75 Ma), expanded into the northern Labrador Sea in the early Paleocene, and ended in the Davis Strait and Baffin Bay during the early Oligocene [*Laughton*, 1971, 1972; *Le Pichon et al.*, 1971; *Hyndman*, 1973, 1975; *van der Linden*, 1975; *Srivastava*, 1978, 1983; *Hinz et al.*, 1979; *Srivastava et al.*, 1980; *Johnson et al.*, 1982; *Srivastava and Tapscott*, 1986]. The

[1]Now at Alfred Wegener Institute for Polar and Marine Research, Bremerhaven, Germany.

Paper number 93JB00016.
0148-0227/93/93JB-00016$05.00

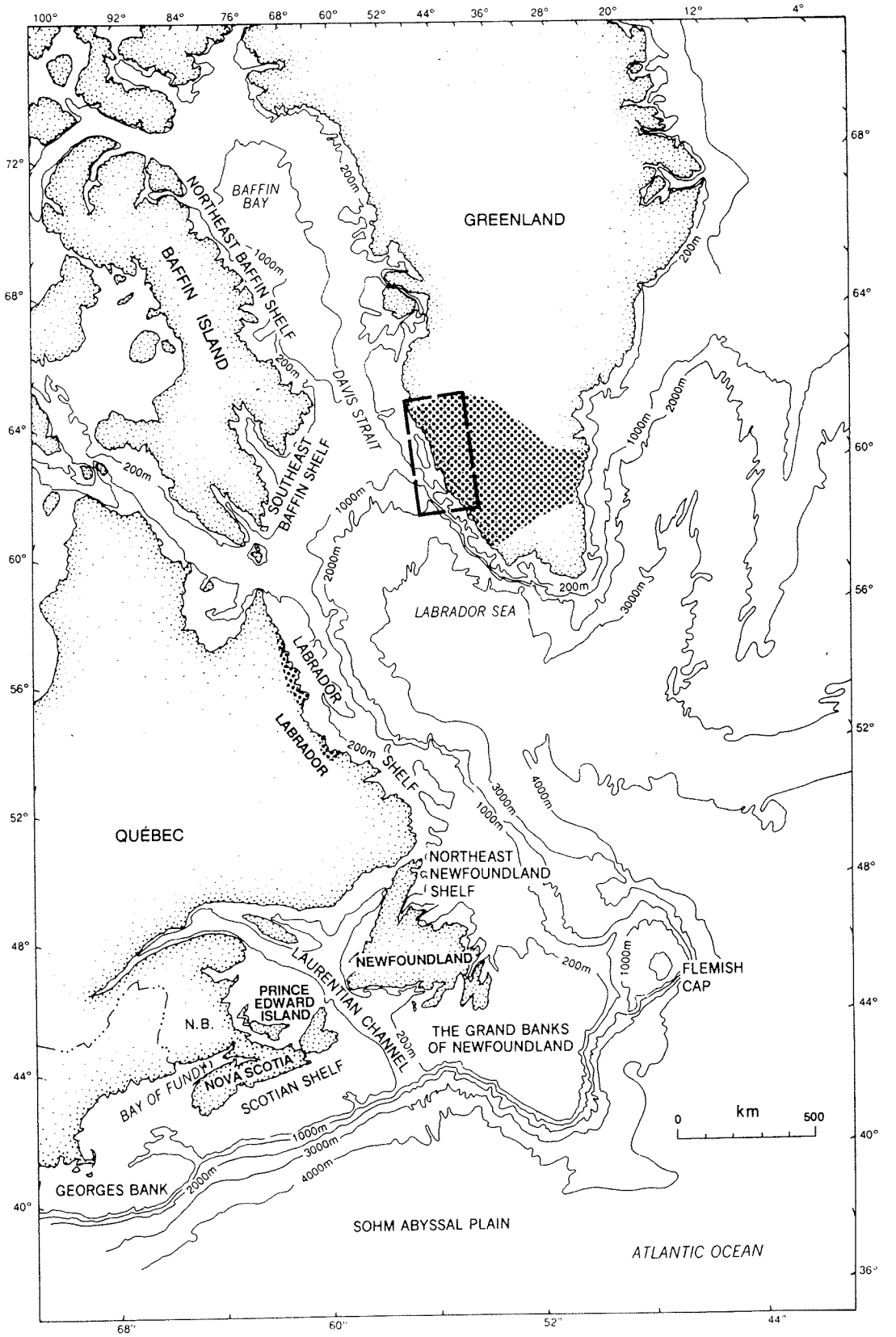

Fig. 1. General map of the northeastern Atlantic region. Greenland rifted from the North American continent between Late Cretaceous and Oligocene time creating a relatively thick oceanic crust of the Davis Strait and northern Labrador Sea. The narrow width of the SW Greenland shelf as opposed to the wider shelf off Labrador indicates asymmetric Labrador Sea margins. Areas of heavy dots illustrate the North Atlantic Archean craton in Greenland and Labrador [after *Bridgwater et al.*, 1973]. The box marks our study area (Figure 2). The coastline and bathymetry map was adopted from *Keen and Williams* [1990] and the Geological Survey of Canada, Department of Energy, Mines and Resources, and reproduced with permission of the Minister of Supply and Services Canada, 1992.

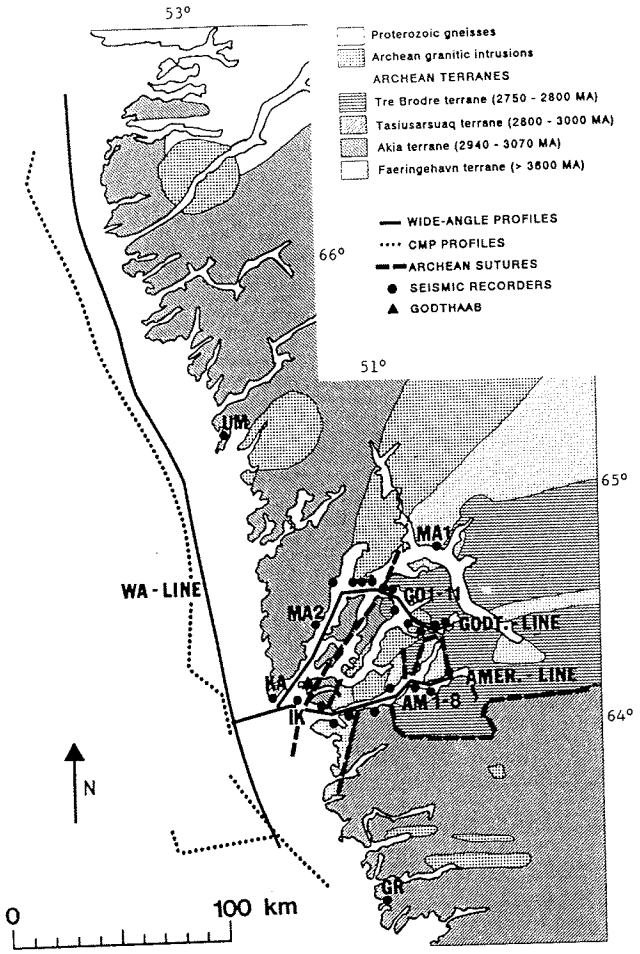

Fig. 2. Map of the general geology of study area in SW Greenland including seismic source and receiver locations. The geologic information is compiled from published maps from the *Geological Survey of Greenland* [1982], *Nutman et al.* [1989], and *Friend and Nutman* [1991]. Three-component seismic instruments located along the coast (UM, KA, IK, GR) and two fjords, Godthåbsfjord and Ameralik (GO 1 to 11, AM 1 to 8, MA 1 and 2) recorded densely spaced air gun shots from profiles WA, GO, and AM. Recordings from coastline profile WA are used in this study.

Labrador Basin is characterized by asymmetric continental margins (Figure 1). The SW Greenland shelf is particularly narrow, being less than 70 km across in the south, and gradually widens northward from the study area to about 230 km width. The Labrador shelf has a width of 110 km to 220 km [*Srivastava et al.*, 1980], widening northward. *Srivastava* [1978] and *Hinz et al.* [1979] observe a steep continental slope along the SW Greenland coast between 60° and 62° N latitude and attribute it to normal faulting. Gravity and magnetic profiles across the Labrador Sea [*Hinz et al.*, 1979; *Thorning*, 1984, 1986; *Geological Survey of Canada*, 1988*a,b*; *Woodside and Verhoef*, 1989] indicate asymmetry of the margins. The gravity field across the Greenland margin shows steeper gradients and higher-amplitude anomalies than that of the Labrador margin and can be associated with a steeply dipping basement and a thin or, in places, nonexistent sequence of shelf sediments [*Hinz et al.*, 1979; *Woodside and Verhoef*, 1989]. Gravity studies of the Godthåbsfjord and Ameralik region reveal a positive seaward gradient of the long-wavelength Bouguer anomaly of approximately 2 mGal/km, indicating a 15-20° slope of the crust-mantle boundary along the shelf [*Speece*, 1992]. Seismic reflection and refraction data across the Labrador shelf show a thick sedimentary wedge, while thin or non-existent sedimentary sequences lie on the Greenland shelf above a strongly faulted acoustic basement [*Hinz et al.*, 1979]. The sedimentary cover thickens northward toward the Davis Strait [*Manderscheid*, 1980]. The basement does not show any major continuous reflections but contains diffractions, possibly caused by steeply dipping normal faults. A new model by *Chalmers* [1991] suggests a continental crust that extends much farther into the northwestern Labrador Sea than previously thought [*Roest and Srivastava*, 1989].

An apparent lack of exposed extensive volcanism along the Labrador Sea margins suggests a nonvolcanic rifting event in the Labrador Sea region [*White and McKenzie*, 1989]. Approximately 500 to 600 km north of our study area, formations of basaltic volcanic rocks with thicknesses of up to 8 km are present on Disko Island and the surrounding area as well as on the conjugate margin on Baffin Island [*Clarke*, 1970; *Clarke and Upton*, 1971; *Denham*, 1974; *Clarke and Pederson*, 1976]. The basalts on either side were extruded at about 61-58 Ma [*Clarke and Upton*, 1971] during spreading of the Davis Strait and Baffin Bay and about 15 m.y. after the initial opening of the Labrador Sea. *Hinz et al.* [1979], however, related the flat acoustic basement on the Labrador shelf and the subbasement reflectors to possible younger basalt flows that overlay pyroclastic or sedimentary sequences on top of a slightly older oceanic crust. Indications of high-velocity zones (v_p > 7.2 km/s) in the lowermost crust of the Labrador shelf [*Hinz et al.*, 1979] and at the bottom of the oceanic crust adjacent to the Greenland margin [*Stergiopoulos*, 1984] further imply a magmatic rift event in the Labrador Sea region. Wide-angle data from the shelf crossing the southern boundary of the Archean block of SW Greenland do not contain evidence for a high-velocity zone at the base of the transitional crust [*Chian and Louden*, 1992]. *Hyndman* [1975] developed a model for the region, in which an active hot spot under the Davis Strait produced volcanism and thickened the crust after sea floor was created. *White and McKenzie* [1989] argue that extensive rift margin volcanism and associated crustal thickening in the Davis Strait were generated by an intersection of the rift with an asthenospheric plume that caused rifting in the North Atlantic and migrated underneath Greenland or that volcanism was caused by a separate hot spot that had been initiated under the Davis Strait.

DATA ACQUISITION AND PROCESSING

A major part of the seismic experiment in SW Greenland was designed to obtain a velocity distribution from a profile (WA) along the NNW-SSE striking shelf (Figure 2). The use of an air gun array permitted the recording of densely spaced, generally unaliased seismic data that allowed accurate correlation of phases and detailed inverse and forward modeling. A source array of five air guns (19.7 L or 1200 cubic inches each) with a peak pressure of 140 bars was fired at 15 m depth at a spacing of 100 to 150 m. For this study, we analyzed recordings of REFTEK PASSCAL 72A digital instruments, situated on four bedrock locations (UM, IK, KA, GR) along the coast (Figure 2). All instruments recorded three components, but we used only the information of the vertical components for this study. Processing of the

horizontal components and a detailed *S* and converted wave study is in progress.

The dominant signal frequency range is between 7 and 9 Hz, with smaller peaks at 15 to 17 Hz and 23 to 25 Hz. We applied a band-pass filter from 7 to 30 Hz with a taper of one octave on either side. Large variations in the alignment of the first breaks are due to datum static shifts. We applied elevation static corrections to all receiver gathers by replacing the water column with a 5.5 km/s velocity layer. This correction velocity corresponds to a velocity of the near-offset first breaks. Also, static corrections to compensate for the air gun depth (correction velocity of 1.5 km/s) and for the instrument elevation (elevations between 8 and 20 m; correction velocity: 5.5 km/s) were applied. The results improved the correlation of dominant phases, although some static shifts remained, particularly in troughs and overdeepened river valleys.

To eliminate bubble reverberations and sea bottom multiples, we applied a predictive deconvolution. An operator of 500 ms length with a gap of 125 ms, corresponding to the second zero crossing of an 8 Hz wavelet, provided the best results in compressing the wavelet (Figure 3). We chose a 5-s design gate, beginning at the first arrival. The operator was then applied to the entire trace. Deconvolution was particularly successful as an aid in seismic phase identification. Phases in close proximity are displayed as distinct arrivals after deconvolution was applied, i.e., the arrivals labeled as P_iP and P_mP (Figure 3).

We filtered near-offset traces in the frequency-wavenumber (FK) domain to remove direct *S* and water waves that interfered with several *P* wave arrivals. We applied a rejection range of 1400-1600 m/s for the water wave noise and 3600-3800 m/s for the direct *S* waves. A previously applied automatic gain control (AGC) of 3 s improved the filtered results because of an improved signal-to-noise ratio (Figures 4*a*-4*b*).

Rejection of direct *S* wave and water wave noise in the intercept time ray parameter (tau-p) domain also improves the signal-to-noise ratio. A comparison with FK filtering shows that more coherent seismic arrivals from the original x-t domain were extracted by tau-p filtering (Figures 4*c*-4*e*). Coherency filtering in the tau-p domain [*Stoffa et al.*, 1981] improves the signal-to-noise ratio but also generates artifacts. We identified seismic phases by comparing FK and tau-p filtered sections with unfiltered data.

We slant stacked [i.e., *McMechan and Ottolini*, 1980; *Diebold and Stoffa*, 1981; *Phinney et al.*, 1981] the receiver gathers to obtain an immediate estimate of the apparent arrival velocities and to identify precritical and postcritical reflections and refractions. The signal-to-noise ratio of arrivals in the tau-p domain is theoretically enhanced by the square root of the number of traces in the stacking process. A muting process can be performed in the tau-p domain to eliminate arrivals within a defined slowness range (i.e., water waves and direct waves). By applying a coherency filter [*Stoffa et al.*, 1981] using semblance calculations, regions with low coherency were zeroed out and aliasing along with other incoherent noise was suppressed.

We split every receiver gather into overlapping windows of about 20-km aperture and transformed each window into the tau-p domain. The coherency-filtered windows of one shot direction with respect to the receiver location were subsequently summed. Splitting the shots into several windows before slant stacking has the advantage of controlling unavoidable averaging effects by transforming data from a large offset range. Each window in the tau-p domain can be interpreted individually which is important in areas of heterogeneity.

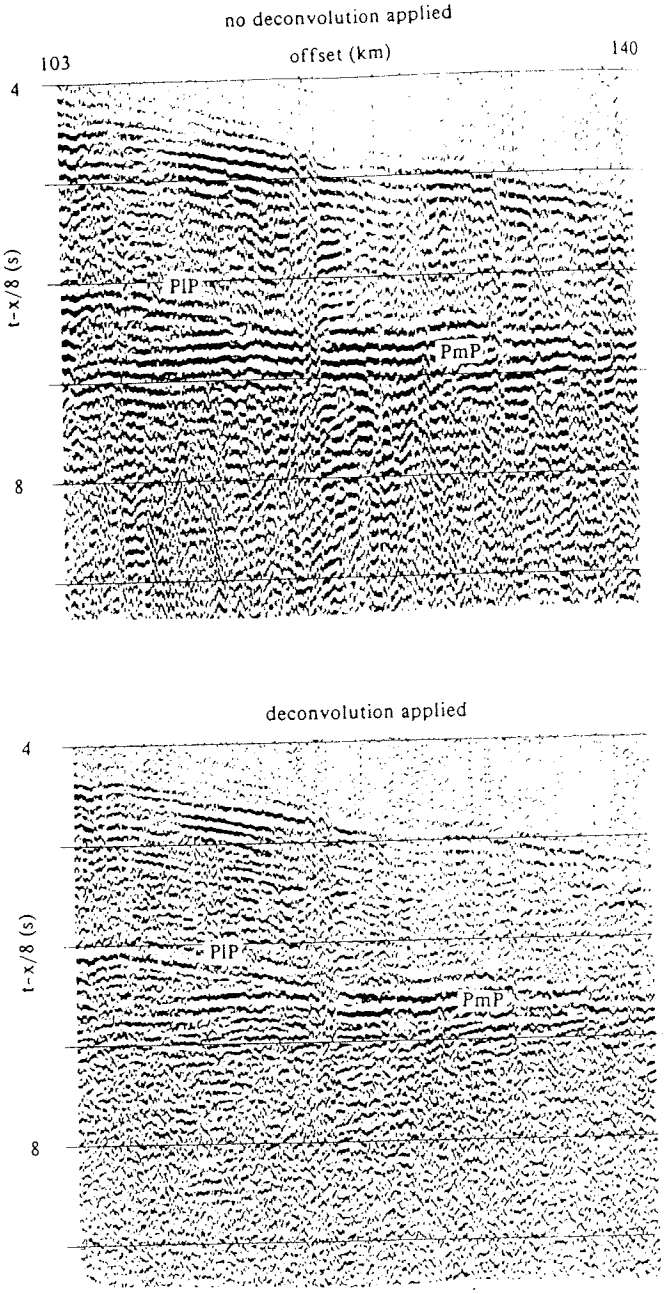

Fig. 3. Seismic section before and after deconvolution. Deconvolution eliminates the bubble reverberations and most of the sea bottom multiples and is, therefore, a valuable aid for identifying phases.

Description of Seismic Phases

The vertical components from the coast stations UM, KA, IK and GR that recorded profile WA contain several middle and lower crustal reflected and refracted *P* wave events (Figures 5*a*-5*d*). The first arrival (P_g) shows highly varying apparent velocities between 5.4 and 7.1 km/s in all receiver gathers,

partly due to remaining static shifts and lateral velocity variations. Midcrustal P wave reflections are very discontinuous in all recordings. Their coherency and amplitudes are low at precritical distances and increase with larger offsets. One of the most prominent features of the vertical component is a strong, continuous lower crustal precritical and postcritical reflection (P_lP) that converges with an equally high-amplitude Moho reflection (P_mP). This convergence is a rare observation in deep crustal seismic recordings; it illustrates the improvement of seismic data quality with dense trace spacing. Despite interruptions of its continuity at precritical distance, the P_lP event is traced to near offsets. The observation of two distinct lower crustal phases (P_lP and P_mP) in the recordings of the northern section of UM (Figure 5*a*) is not as obvious as it is for KA and IK. A strong P_lP phase follows continuously through the section into the coherency-filtered near-offset range. The P_mP phase appears at offsets greater than 60 km . Within the southern section of recording UM (Figure 5*b*), both phases converge at 100 km distance.

Station IK recorded an upper mantle refraction (P_n) with an apparent velocity of 8.1 to 8.3 km/s. A portion of that phase can be seen through the reverberations and coda of the first arrival between offsets of 140 to 160 km (Figure 5*d*).

Plots of coherency-filtered and vertically stacked slant stacks show strong P wave arrivals (Figure 6) that we correlated with arrivals of the respective time-offset gathers. The P_g phase consists of several high-amplitude clusters between ray parameters 0.185 and 0.140 s/km (apparent velocities of 5.4 and 7.1 km/s) corresponding to variations in the first-break alignment of the offset gather. Several midcrustal phases show strong amplitudes from critical to postcritical angles, indicated by their ray parameters of 0.160 to 0.140 s/km (apparent velocities of 6.3 to 7.1 km/s). Locally dipping structures possibly generated smearing effects of midcrustal phases in recording GR which makes an identification difficult. Tau-p gathers of stations UM, IK, and KA show clear images of precritical and postcritical reflections from the lower crust and Moho. The P_lP and P_mP phases appear as high-amplitude events, corresponding to the relatively high energy returning from those interfaces at critical and postcritical distances.

INVERSION

1-D Inversion

As a preliminary step in the interpretation of the densely spaced wide-angle reflection data from the coast line

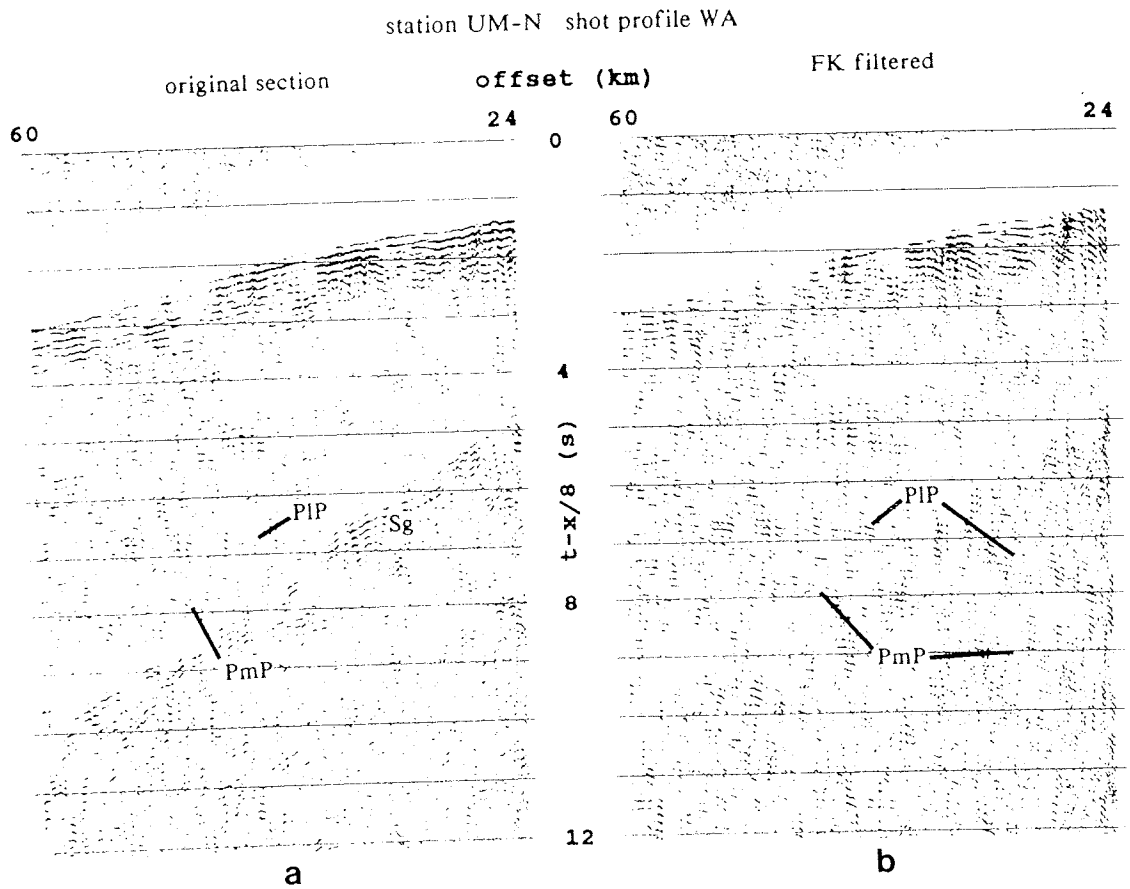

Fig. 4. Elimination of near-offset S wave noise, (*a*) without coherency filter, (*b*) with coherency (FK) filter. P_lP and P_mP phases appear at smaller offsets after elimination of most direct S wave arrivals. (*c*) By transforming the offset data into the tau-p domain, muting and coherency filtering in the tau-p domain, and transforming back into the time-offset domain, arrivals are enhanced. (*d*) A coherency filter in the tau-p domain uses the semblance calculation [*Stoffa et al.*, 1981] with different thresholds for noise rejection. (*e*) The lower the threshold the more noise, and eventually signal, is rejected. Isolated events of high-amplitude noise in the tau-p domain may transform back as linear events that should not be confused with seismic arrivals.

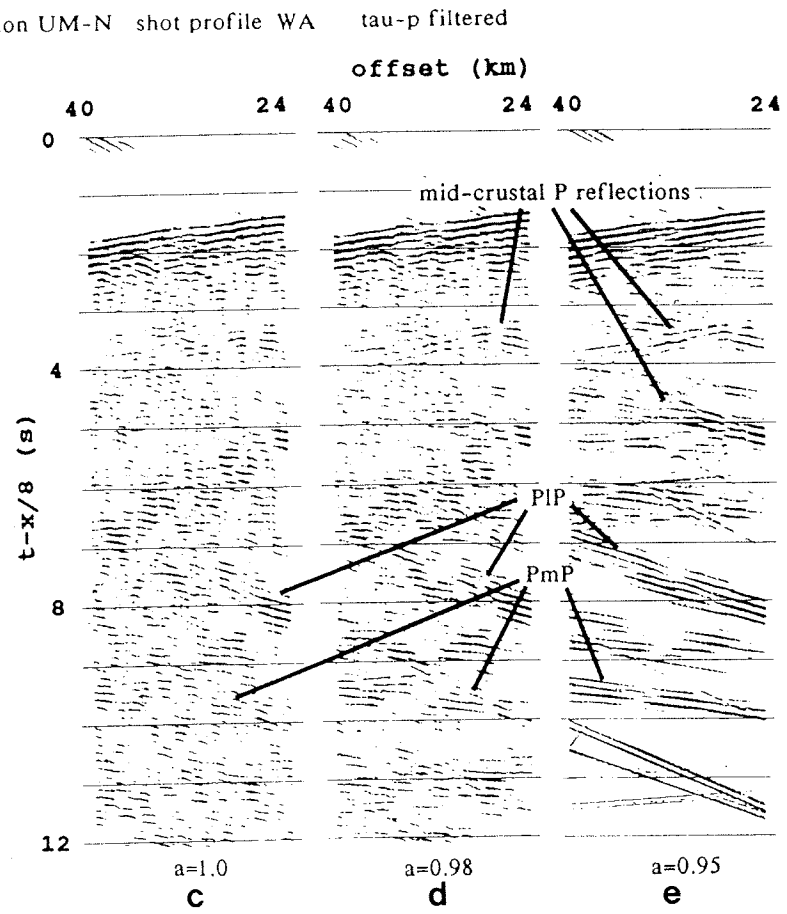

Fig. 4. (continued)

recordings, we performed an inversion of individual receiver gathers to estimate local depth bounds for the equivalent 1-D structure [*Gohl et al.*, 1991]. Although the bounds are biased to some extent by local dip effects, the inversion results provide useful starting values for deriving more realistic models. We used an extremal inversion method [*Bessonova et al.*, 1974; *Hawman and Phinney*, 1991] based on picks in the tau-p domain to invert for minimum and maximum depths of horizontal layers of constant slownesses. Picks in the tau-p domain were made at the onset of each arrival. Uncertainties assigned to intercept-time picks were based on the signal bandwidths [*Kennett and Orcutt*, 1976] and the S/N ratio of the arrivals but did not incorporate scatter due to local dip effects. These uncertainties ranged between 0.08 and 0.20 s. We parameterized the model as a stack of layers of constant slownesses (slowness increment is 0.001 s/km) with slownesses decreasing (velocities increasing) with depth. The slowness for the uppermost layer was chosen from the near-offset first break velocities. The minimum slowness was chosen to allow for the possibility of high velocities near the base of the crust. We used tau-p picks from refracted as well as precritical and postcritical reflected phases. By choosing as many precritical and postcritical reflections from a single interface as possible, the depth bounds are better constrained. The extremal method produced a 1-D inverse model (Figure 7) that incorporates data from a large offset range. Several midcrustal discontinuities appear with varying depths, indicating a complex structure with lateral inhomogeneities at midcrustal levels along the recording mid-points. A first-order discontinuity or a strong, narrow gradient zone, 6 to 8 km above the Moho, is derived from the strong, coherent P_lP phase from stations KA and IK. The inversion results infer a crustal depth of 30 to 40 km, increasing northward. The uppermost crust contains a high-velocity gradient. Velocities exceed 6.0 km/s below depths of 4 to 6 km for most recordings, but the gradient remains low for the remainder of the crust. The bottom of the crust consists of a zone with velocities between 7.2 and 7.8 km/s.

The shot profile is located on the shelf parallel to the passive continental margin where the crust-mantle boundary becomes shallower toward the oceanic crust. Therefore, the results of the inversion are biased by a slope of the Moho perpendicular to the profile [*Larkin*, 1992]. However, results from extremal inversion place useful constraints on starting models for more complete analyses in terms of 2-D and 3-D structure.

2-D Inversion

The 2-D travel time inversion used in this study is a fast generalized linear inversion that provides estimates of model parameter uncertainties, resolution, and nonuniqueness [*Zelt and Smith*, 1992]. The iterative character of the method involves forward steps of the inverse approach, such as a ray tracing algorithm [*Zelt and Ellis*, 1988] and an adjustment of model parameters by applying a damped least squares inversion of travel times [*Zelt and Smith*, 1992]. The model

for the inversion is parameterized as a set of layers broken into trapezoidal blocks with velocities and depths defined for each corner. Block boundaries are smoothed to avoid scattering and focussing of ray paths. Takeoff angles for ray tracing are calculated automatically. A damped least squares method is used to update the boundary and velocity nodes for each iteration. The algorithm can perform simultaneous velocity and boundary inversion. To quantitatively evaluate the best iterated model, RMS travel time residuals and parameter resolution are calculated allowing an estimation of the model reliability to be made with respect to the data. The stability of the inversion scheme is increased by reducing the number of independent model parameters, i.e., by keeping the velocity gradient or thickness of a layer fixed or by maintaining a constant velocity discontinuity at a layer boundary, if there is evidence for that in the data. To increase

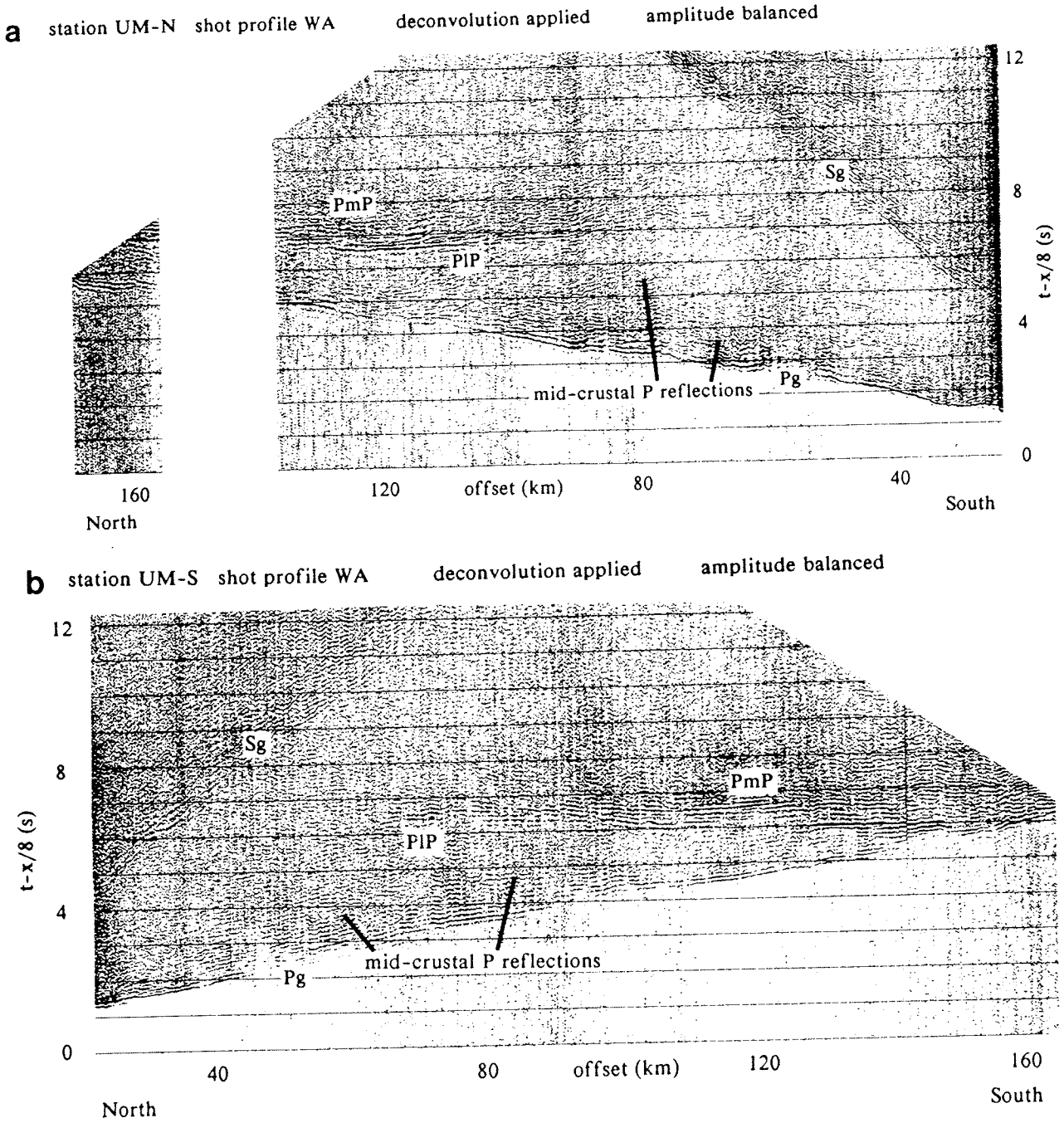

Fig. 5. Receiver gathers of WA profile. Shown are the vertical components with deconvolution applied. (*a*) UM-North, (*b*) UM-South, (*c*) KA, (*d*) IK. Note the high-amplitude lower crustal (P_lP) and Moho (P_mP) arrivals in all recordings. Note that the P_lP phase in some recordings (i.e., KA) can be traced throughout precritical distances to small offsets, an indication for a high impedance contrast in the lower crust. Several midcrustal reflections are identified, but they are weaker and less continuous than the P_lP and P_mP phases. Station KA contains a high-amplitude S_lS or S_mS phase. A P_n phase is observed in recording IK.

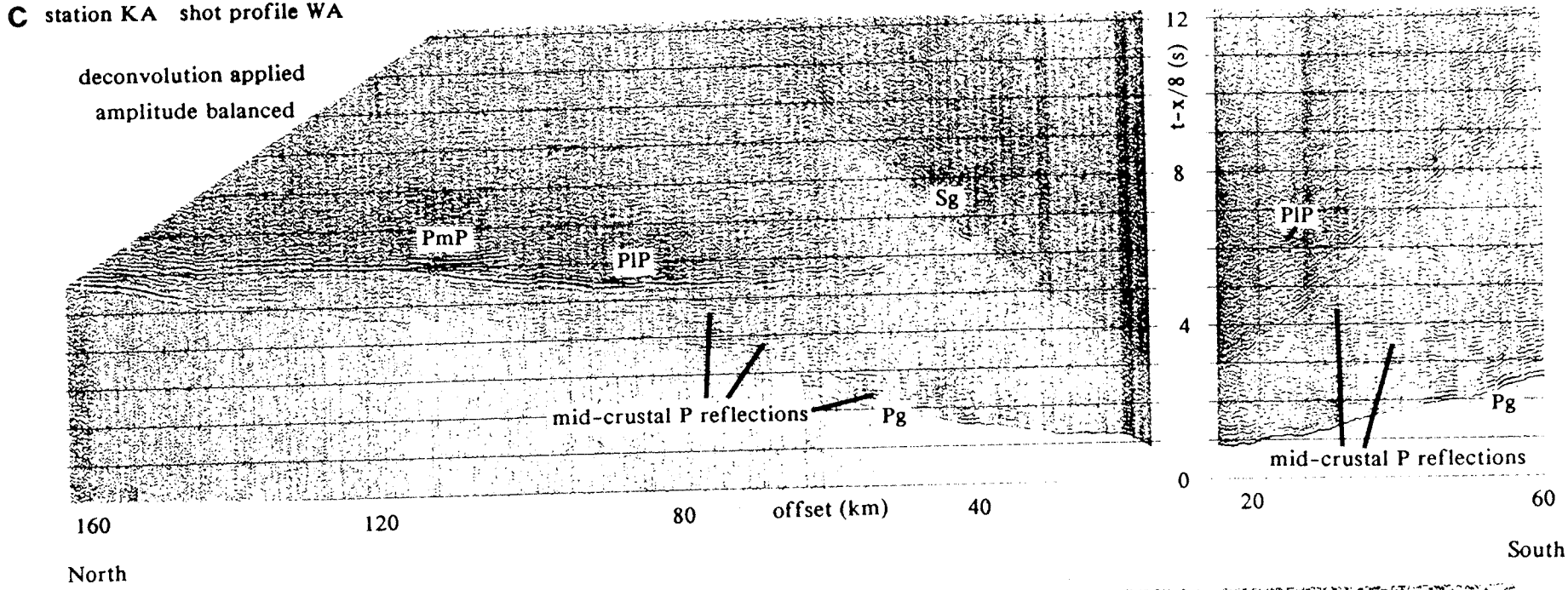
C station KA shot profile WA
deconvolution applied
amplitude balanced
PmP
PlP
Sg
mid-crustal P reflections
Pg
12
8
4
0
t-x/8 (s)
160
120
80
offset (km)
40
North
PlP
Pg
mid-crustal P reflections
20
60
South

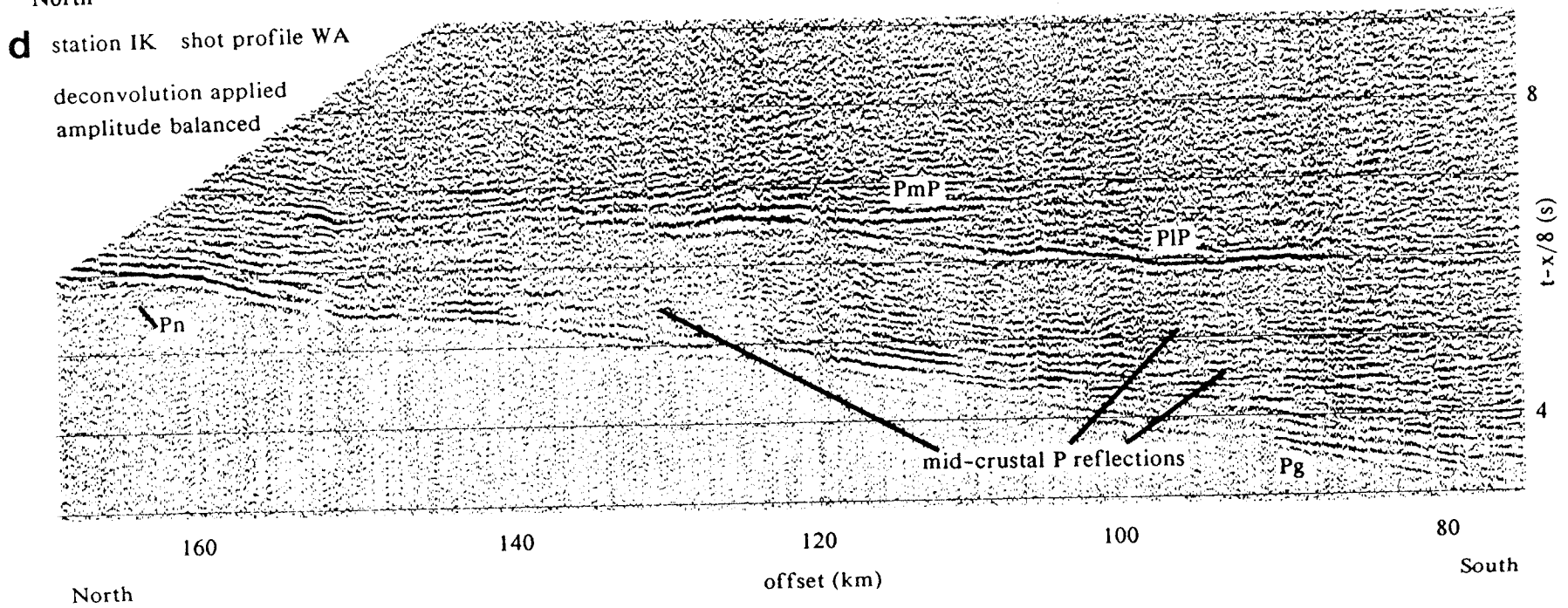
d station IK shot profile WA
deconvolution applied
amplitude balanced
PmP
PlP
Pn
mid-crustal P reflections
Pg
8
4
t-x/8 (s)
160
140
120
100
80
offset (km)
North
South

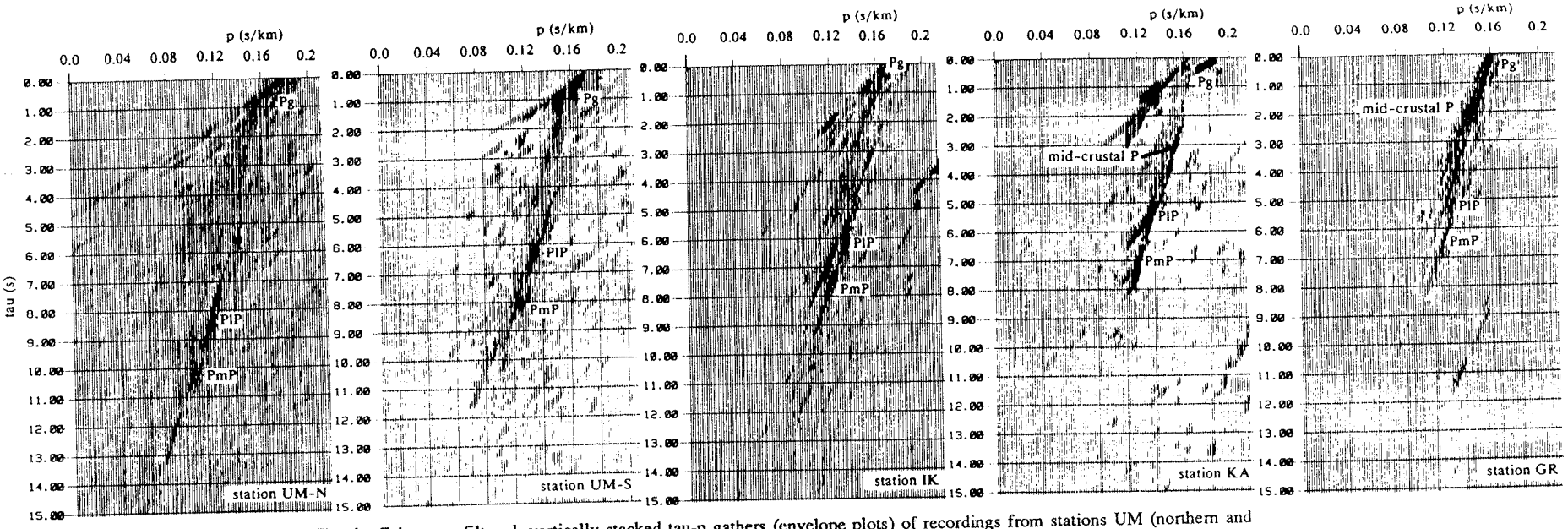

Fig. 6. Coherency-filtered, vertically stacked tau-p gathers (envelope plots) of recordings from stations UM (northern and southern direction), IK, KA, and GR. Recordings UM, KA, and IK contain high-amplitude P_lP and P_mP arrivals. The strongest midcrustal phases appear in recordings KA and GR, indicating localized midcrustal discontinuities.

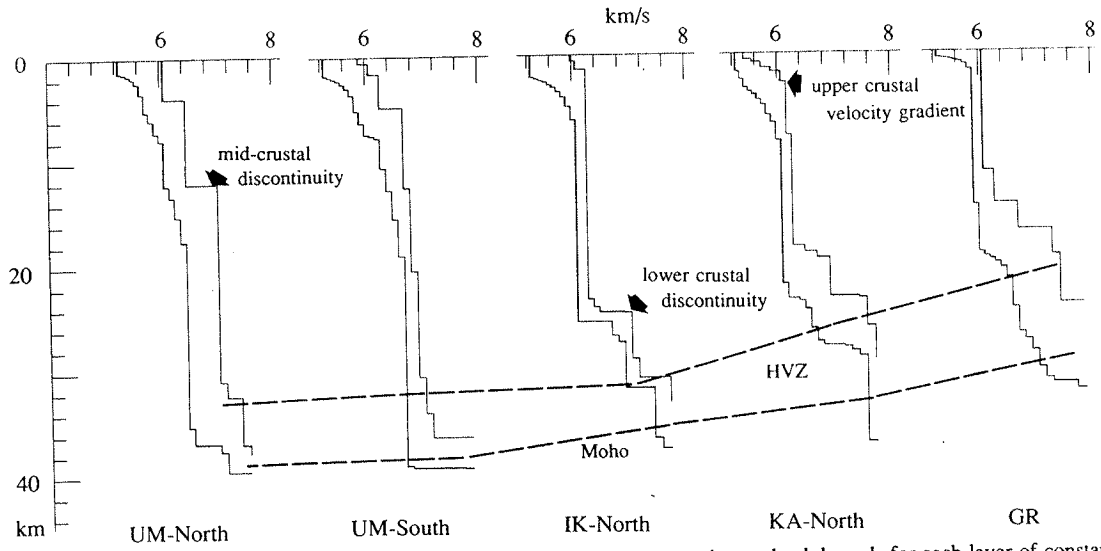

Fig. 7. Results of 1-D extremal inversion. Curves illustrate minimum and maximum depth bounds for each layer of constant slowness. Slowness is displayed as layer velocity. Note the decrease in crustal thickness from station UM to station GR, north to south. A high-velocity zone (HVZ) is illustrated by stippled lines. Inversion models of stations KA and IK show the best indication for a HVZ (>7.2 km/s) above the Moho. Station IK is located farther inland and shows a deeper crust and a thinner HVZ.

stability, we first inverted for the uppermost crust, then continued with arrivals from the middle and lower crust, keeping the parameters of overlying layers fixed.

Profile WA runs parallel to the strike direction of the continental margin. The crustal structure is not strictly two-dimensional, and this will introduce a bias in 2-D modeling. Although 3-D modeling would be more accurate, we attempted a 2-D inversion for various reasons. The observation of continuous, high-amplitude lower crustal and Moho arrivals suggests a laterally continuous lower crustal feature that can be modeled in terms of its velocity and thickness. The large offsets, over which these arrivals can be observed, range from near-vertical to postcritical and place contraints on the velocity estimation. Although calculations of layer depths are biased by the eastward dipping geometry of seismic interfaces within the thinned crust, we can estimate a general trend of N-S dipping structures. We did not include arrivals from receiver IK despite their good quality, because this station is located too far off the profile line.

An initial crustal model was created based on the results from the 1-D tau-p inversion. The model included a northward dipping crust-mantle boundary, with its greatest dip in the southern half of the model, a high-velocity zone at the bottom of the crust and three midcrustal interfaces with small velocity discontinuities and layers of small velocity gradients. As a first approach, we modeled each series of observed travel time arrivals by iterative inversion. The model was parameterized with six layers, and the number of boundary nodes was kept constant for a distance increment of 40 km, except for the northernmost part of the model where the increment was increased to 80 km for the lower layers 2 to 6 due to the lack of observable arrivals. We then corrected the inversion results by manual smoothing and straightening of layer boundaries that were obviously affected by the line geometry. It soon became clear that local dipping structures or interfaces were derived from individual travel time curves at small offsets. Near-offset arrival curves whose hyperbola caused bending of interfaces that could not be constrained from other stations were rejected thereafter to allow rays to travel to the next interface correctly.

After we completed the inversion for all *P* wave arrivals in recordings UM, KA, and GR, the final inversion model served as a highly improved starting model for the next series of iterations. This time, we corrected nodes with unrealistically low or high velocities manually and kept them fixed during subsequent iterations. Also, the number of velocity nodes was increased for layers in which large-offset recordings suggested a variable interface depth, such as the boundaries for layers in the southern half of the model. Most travel time branches match the observed data for further offsets (Figures 8*a*-8*c*).

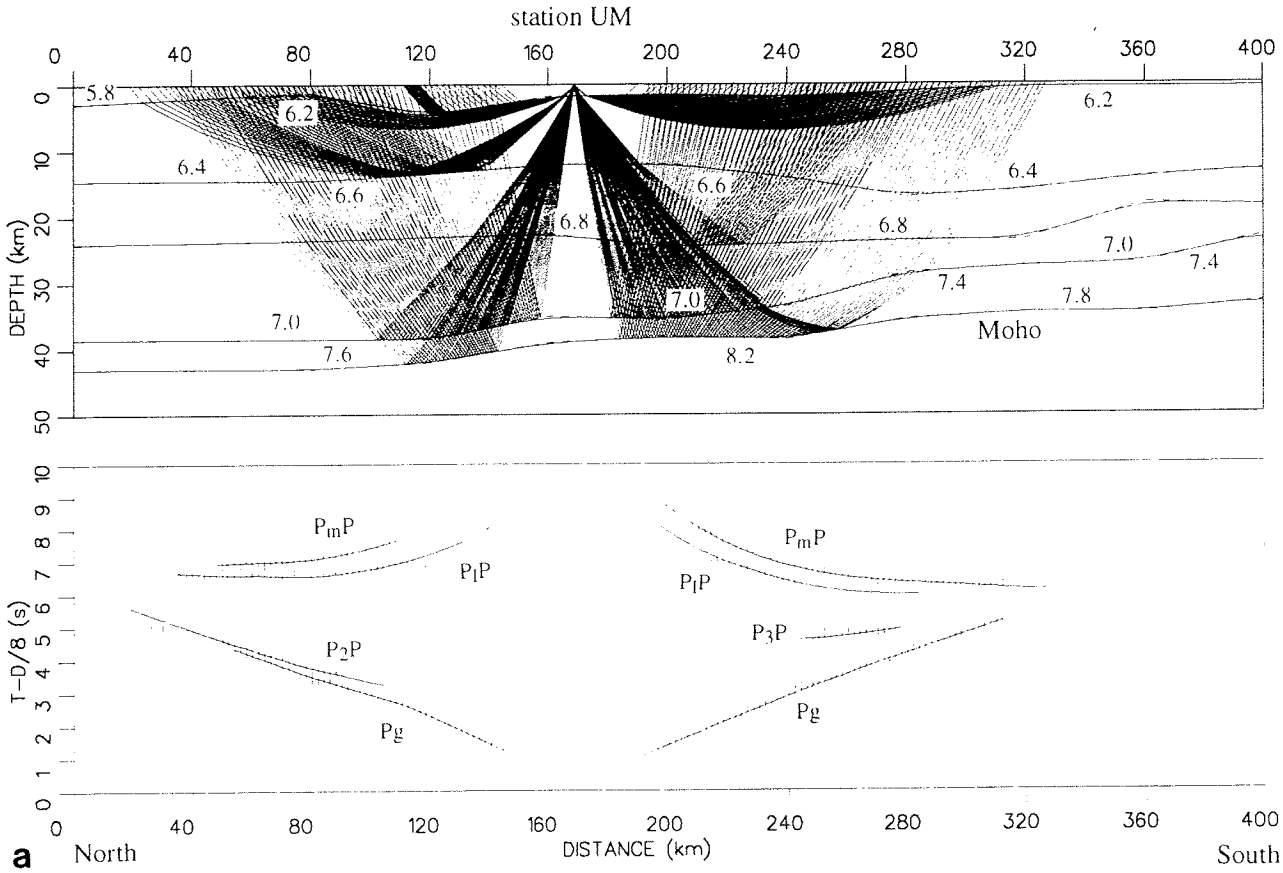

Fig. 8. 2-D travel time forward and inverse model for profile WA. (*a*) UM, (*b*) KA, (*c*) GR. Rays were shot through the final model. Heavy lines represent observed travel times, with width indicating uncertainties in phase picking. Thin lines illustrate calculated travel times. *P* wave velocities (km/s) and phase labels are included. The distance axes are related to absolute distance of model profile (0-400 km). Although more midcrustal reflections are observed in the data, only those that could be correlated over, at least, two stations were included in the inversion.

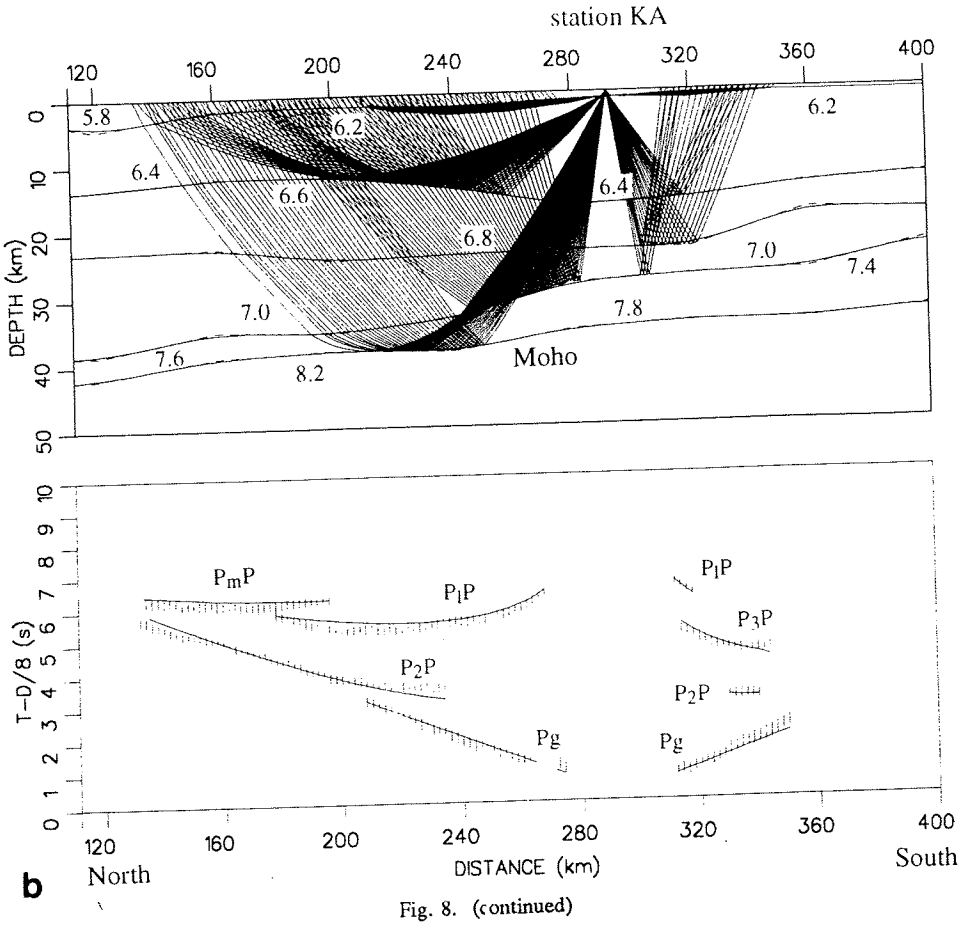

Fig. 8. (continued)

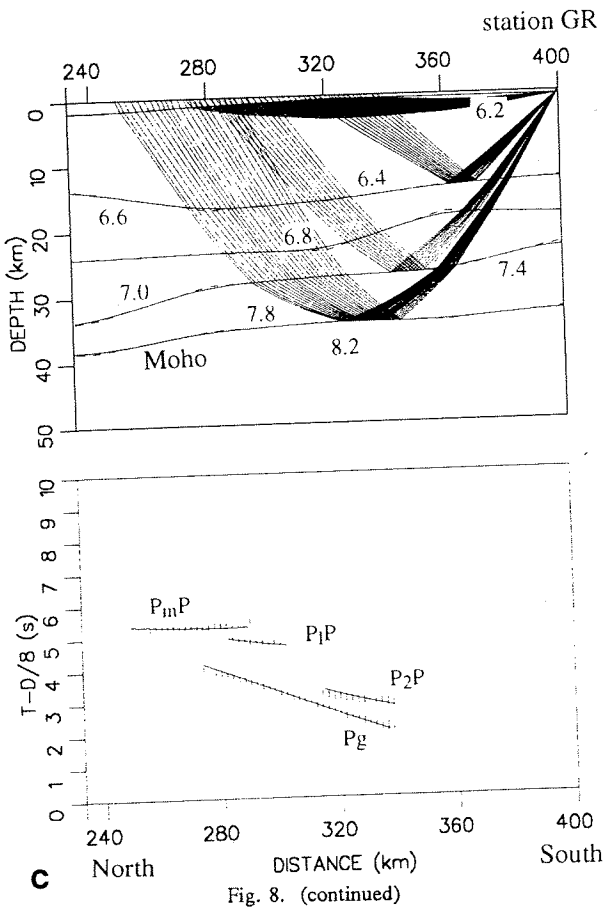

Fig. 8. (continued)

In the final model, we matched the majority of travel time picks by rejecting near-offset arrivals that were most influenced by the fan geometry (Figures 9 and 10*a*). The data do not show evidence for a thick low-velocity sedimentary sequence. A large vertical velocity gradient exists within the uppermost crust, with velocities increasing to 6.3 km/s within 1 km from the surface (Figure 9). First-arrival *P* wave velocities of 6.3 to 6.5 km/s represent velocities of the upper crust to about 12 km depth. Upper crustal zones having lower velocities (i.e., 5.8 km/s at 120 km distance and 4.5 km depth) correspond to areas of poor resolution (Figure 10*b*). Between 12 and 25 km depth, the velocities increase from about 6.5 km/s to 6.8 km/s (Figure 10*a*). A continuous high-velocity zone with a thickness of 3 to 8 km and a velocity of 7.4 to 7.7 km/s, increasing with depth, is defined by the continuous P_1P and P_mP phases. Due to lack of refracted arrivals travelling through the lowermost layer, we relied on the relative move-outs of P_mP to derive velocities. To test the reliability of the velocities in the lowermost layer, we replaced the velocities of this layer with a variety of initial velocities ranging from 6.9 to 7.7 km/s (average velocity) and applied the damped least squares inversion over several iterations. The initial velocities converged to a final average velocity of about 7.5 km/s after 3 or 4 iterations. Initial velocities below 6.9 km/s resulted in an unstable inversion. Table 1 illustrates that RMS travel time residuals and χ^2 values reached their minima at an average velocity of the HVZ of 7.5 to 7.6 km/s, showing that the error between calculated and observed travel times is minimized with this average velocity. The result of this test places confidence in the modeled

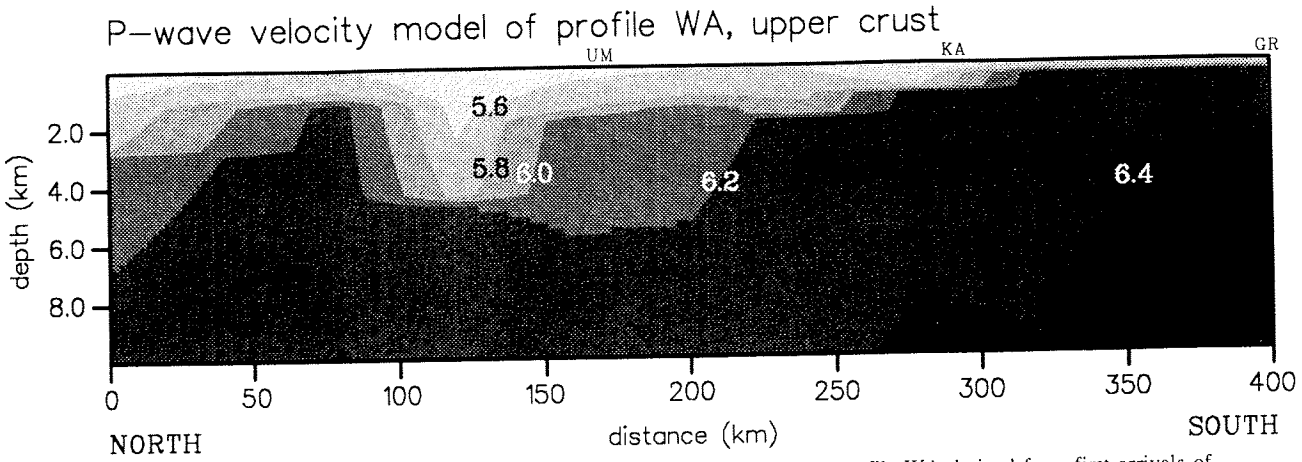

Fig. 9. Two-dimensional *P* wave velocity/depth model of the upper crust along profile WA derived from first arrivals of recordings UM, KA, and GR. The numbers correspond to *P* wave velocities (km/s) along contour lines.

velocities of the lowermost layer which will be crucial for our interpretation.

The Moho depth reaches 30 km in the southern part of the profile and increases northward to about 42 km. The northward deepening of the crust along the coast is in agreement with a gravity study by *Speece* [1992].

Resolution of 2-D Inversion

One advantage of using an inversion routine is the ability to calculate the resolution of the model parameters. The diagonal elements of the resolution matrix range between zero and one. The calculated uncertainty of individual velocity and

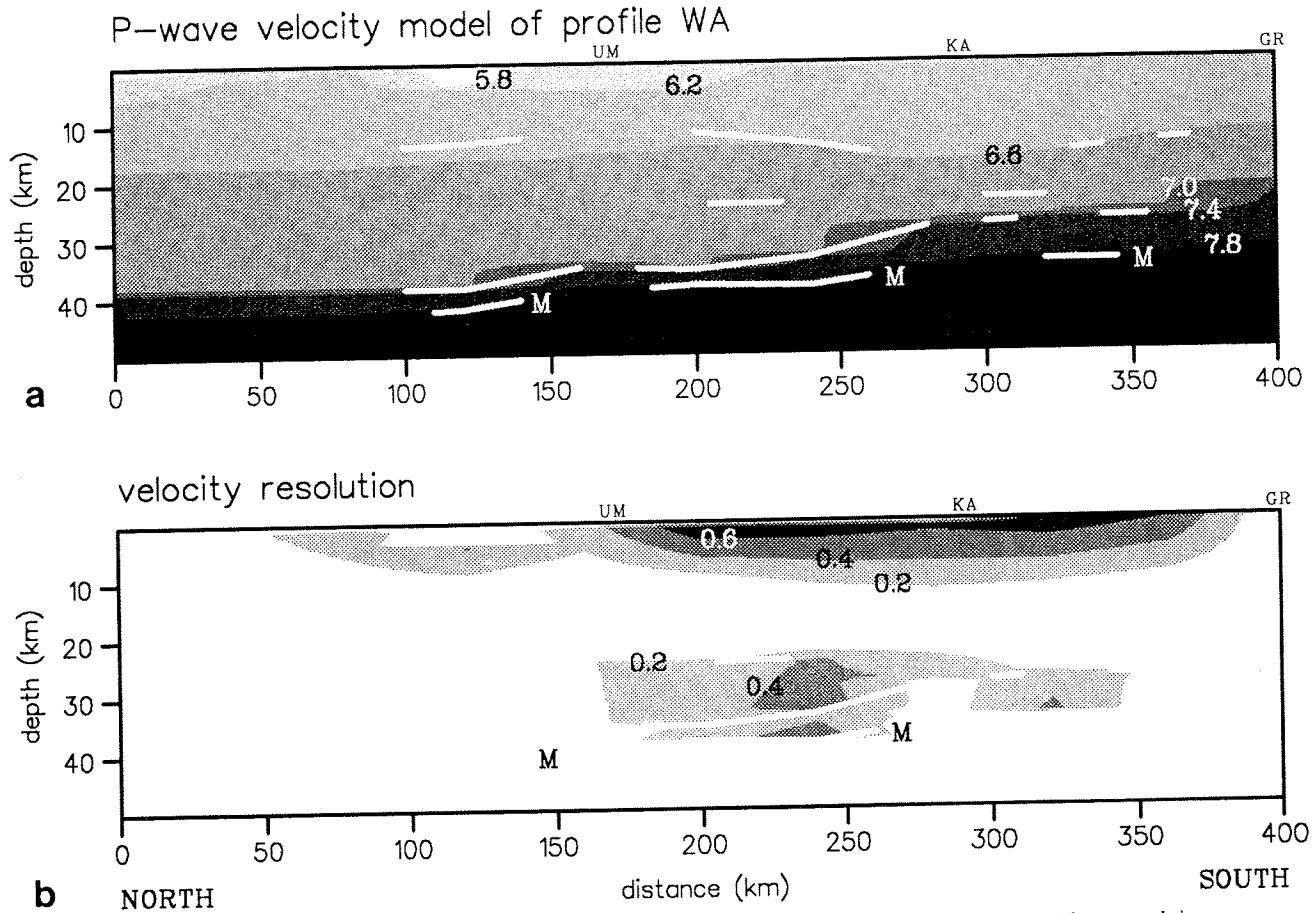

Fig. 10. (*a*) Final 2-D *P* wave velocity/depth model and (*b*) velocity resolution plot for profile WA derived from travel time forward and inverse modeling. Because of 3-D effects, the inversion of arrivals was manipulated so that near-offset arrivals were ignored and oscillations of interfaces due to interpolated arrivals were straightened. The numbers correspond to *P* wave velocities (km/s) and resolution values ($0 \leq R \leq 1$) along contour lines. White lines illustrate wide-angle reflectors with a depth resolution of larger than 0.5. The projected receiver locations are annotated by UM, KA, and GR. The white zones mark areas without any ray coverage. Note that velocities are better resolved in the upper crust and portions of the lower crust in which overlapping ray coverage exists. The high-velocity zone (HVZ) at the bottom of the marginal crust is constrained by the relative move-out of P_mP phases.

TABLE 1. Range of Average P Wave Velocities V_{av} to Illustrate the Velocity Reliability for the Lowermost Layer

V_{av}, km/s	N	T_{RMS}, s	χ^2
6.9	297	0.33	7.03
7.0	297	0.30	5.77
7.1	299	0.26	4.28
7.2	298	0.22	3.03
7.3	297	0.19	1.97
7.4	297	0.16	1.28
7.5	299	0.13	0.87
7.6	290	0.13	0.81
7.7	291	0.16	1.24

N annotates the number of P_mP travel time observations used. Minima of RMS travel time residuals T_{RMS} and normalized χ^2 are reached with an average velocity between 7.5 and 7.6 km/s.

boundary nodes is obtained by taking the square root of the diagonal elements of the covariance matrix [*Zelt and Smith*, 1992]. This quantitative calculation is best used in a relative rather than absolute sense and does not take into account 2-D modeling of a 3-D structure, misidentification of phases, and a coarse block parameterization of the model through neglecting fine heterogeneities [*Zelt and Smith*, 1992]. We calculated the resolution of the nodes in our final velocity/depth model to obtain an image of the distribution of resolution kernels within the model. The velocity and depth resolution depends on how each node is controlled by a relative number of rays. Therefore, nodes with low ray coverage have low resolution and vice versa. Velocity nodes that are controlled by a high number of refracted or diving rays from more than one location of origin have a good resolution. The resolution of boundary nodes is best constrained by reflected phases within the corresponding layer.

Our model P wave velocities (Figure 10*b*) are well resolved in the southern half of the upper crust and in distinct zones in the lower crust. The small number of stations parallel to the profile and lack of refracted midcrustal and lower crustal arrivals limit the extent of well-resolved velocities. Reflector depths, however, are better constrained given the trade-off between velocity and depth. The depth resolution for reflectors shown in Figure 10*b* ranges between 0.4 and 0.9 (uncertainty < 1 km). Velocity resolution kernels for layers with overlapping refracted (or diving) rays lie between 0.3 and 0.75 (uncertainty < 0.15 km/s). The velocities in the lower crust are controlled by overlapping and reversed rays of the P_lP and P_mP phases and contain resolution kernels of up to 0.5 (uncertainty < 0.1 km/s). Numerical calculation of uncertainties shows that modeled velocities derived from overlapping rays of reflected wide-angle phases can be well resolved without information from refracted waves. Due to the sparse station spacing, high-velocity resolution is limited to two zones within the HVZ. Both zones exhibit similar velocities. Therefore, we suggest that these well-resolved velocities are representive for the modeled HVZ along profile WA.

Comparing 1-D and 2-D Inversion Results

We next compare results from the 1-D extremal inversion (Figure 7) with the 2-D travel time inversion model (Figure 10*a*). As mentioned above, the recordings of station IK were not included in the 2-D modeling process because of its location farther inland over thicker crust than station KA. The depth bounds of dipping lower crustal and Moho discontinuities appear 3 to 5 km shallower in the 1-D models of recordings GR, KA, and UM-North where the receiver gather is located in down dip direction. Lower apparent velocities and lower intercept times of arrivals force the 1-D inversion to shallower depths. The opposite effect is the case in recording UM-South where the shot spread lies in up dip direction of the Moho boundary. Here, the crustal depth of the reflection midpoints derived from the 1-D inversion is 1 to 2 km greater than in the 2-D model (36-38 km). The high velocities of 6.9 to 7.7 km/s for the lower half of the crustal 2-D model lie within the bounds of the 1-D models. We can conclude that inverting for 1-D velocity-depth bounds provides useful and objective initial boundary and velocity nodes for a 2-D inversion. One-dimensional models from several stations along dipping structure can provide estimates of dip angles.

INTERPRETATION AND DISCUSSION OF MODELING RESULTS

Structure and Composition of the Margin

Inverse and forward modeling of the wide-angle data reveal new results concerning the structure and composition of the thinned or transitional Archean crust in SW Greenland. The portion of the crust close to the passive margin is highly affected by the Labrador Sea rifting event. The crust contains numerous moderate and high-amplitude lower crustal reflections both at near and far offsets, suggesting large impedance contrasts, possibly related to emplacement of high-velocity mafic rocks from the mantle during rifting. The thinned crust beneath the shelf has a more mafic composition than the Archean continental crust of SW Greenland, indicated by a higher average crustal velocity of about 6.6 ± 0.1 km/s as opposed to about 6.3 ± 0.1 km/s for the continental crust [*Larkin*, 1992]. An addition of 20% mafic rock (7.3 km/s) into the upper 20 km of a 40-km-thick crust and an addition of 50% mafic rock into the lower 20 km, assuming preexisting average velocities of 6.1 km/s for the upper 20 km and 6.5 km/s for the lower 20 km, would increase the total average crustal velocity from 6.3 to 6.6 km/s. Midcrustal reflections might originate from intruded and elongated mafic bodies emplaced during an early stage of rifting, possible shear zones developed as a result of extension, or from mafic rocks in the original Archean crust. Seismic studies of metamorphic core complexes in the Basin and Range include interpretations where a combination of mafic intrusions and extensional processes might account for high-amplitude reflection zones in the midcrustal area [*McCarthy and Thompson*, 1988].

The most prominent feature of the crust beneath the shelf is a high-velocity zone, up to 8 km thick, at the bottom of the crust. The results of two independent inversion techniques place confidence in the velocity range of 7.4 to 7.7 km/s. This zone exists only within the thinned continental or transitional crust and not at the bottom of the continental crust farther inland [*Larkin*, 1992], indicating its probable association with rifting processes. The high velocities within that zone could be caused by mafic to ultramafic rocks that were intruded or underplated [*Furlong and Fountain*, 1986; *Fountain*, 1989]. These velocities are higher than those of the lowermost transitional crust of the eastern U.S. and Canada [*LASE Study Group*, 1986; *Reid and Keen*, 1990*b*].

The 7.2 km/s layer of the eastern United States continental shelf is interpreted as being made of plutonic gabbroic rocks [*LASE Study Group*, 1986]. High-pressure laboratory velocity measurements of rock samples from the exposed lower crustal Ivrea zone reveal *P* wave velocities from 7.2 to 7.5 km/s for metagabbro and from 7.4 to 7.6 km/s for mafic granulite at room temperature [*Burke and Fountain*, 1990]. These velocities were measured between 600 and 1000 MPa (6 and 10 kbar), corresponding to a depth of 20 to 35 km. Amphibolites and pyroxenites can exhibit *P* wave velocities between 7.0 and 7.7 km/s at 600 to 1000 MPa, especially if they contain garnet [*Christensen and Fountain*, 1975; *Fountain*, 1976; *Burke and Fountain*, 1990; *Fountain et al.*, 1990]. Based on theoretical calculations of compressional rock velocities with respect to pressure and temperature, *Furlong and Fountain* [1986] estimate that underplated olivine-gabbro can reach *P* wave velocities of up to 7.8 km/s at 35 to 40 km depth assuming an intermediate surface heat flow of 60 mW/m^2. *Kern and Richter* [1981] measured the effect of temperature on seismic velocities. They calculated temperature derivatives between -1.6 and -4.9 x 10^4 km/s °C for a variety of rock samples under 600 MPa pressure. Gneisses, amphibolites, and eclogites exhibit temperature derivatives of only -1.6 to -3.0 x 10^4 km/s °C. By assuming a geotherm corresponding to a surface heat flow of about 50 mW/m^2 with respect to a thinned continental crust (extension factor of about 1.5) 80 Ma after the initial rifting event [*McKenzie*, 1978], our observed lower crustal velocities need to be increased by 0.07 to 0.15 km/s for comparison with lab measurements at room temperature. These temperature-corrected velocities, between 7.5 to 7.85 km/s, exceed the range of most observed laboratory data with the exception of eclogite but lie within the calculated velocity range of intermediate velocities appropriate for lowermost crustal and uppermost mantle materials [*Furlong and Fountain*, 1986]. Considering the great depth of the marginal crust of SW Greenland, it is likely that most of the magmatic underplate underwent metamorphism to garnet-pyroxene-granulite facies during cooling.

Implications for Evolution of the Labrador Sea

High-velocity layers at the bottom of the thinned or transitional crust are observed on several passive margins [*Weigel et al.*, 1982; *LASE Study Group*, 1986; *Keen and de Voogt*, 1988; *Tréhu et al.*, 1989; *Austin et al.*, 1990; *Reid and Keen*, 1990*a,b*]. *Chian and Louden* [1992], however, do not observe such a zone at the bottom (28 to 30 km depth) of the thinned (?) continental crust of the SW Greenland shelf approximately 500 km south of our profile. Our profile with an up to 8 km thick HVZ is located in the proximity of the Davis Strait where volcanic rocks cover large areas around Disko Island. That implies that a magmatic layer might have been emplaced at the bottom of the crust during "active" rifting of the northern Davis Strait and Baffin Bay due to hot spot activity but did not reach into the central and southern Labrador Sea. *White and McKenzie* [1989] assumed that the Labrador Sea region underwent "passive" rifting with no major magmatism associated, due to the lack of volcanics in SW Greenland and Labrador. Our observation of a thick HVZ indicates that major magmatism occurred about 500 km south of the Disko Island volcanics. A large volume of mantle-derived material must have been added to the crust, without being extruded. The high velocities of 7.5 to 7.85 km/s (temperature-corrected) suggest that the density of the igneous rocks is intermediate between that of continental crust and mantle.

Hinz et al.'s [1979] observation of possible flood basalts on the Labrador shelf and the lack of extruded mafics on the SW Greenland shelf might suggest an asymmetric structure of both conjugate margins similar to the passive margin geometries described by *Lister et al.* [1986, 1991]. This suggestion is supported by the existence of a magmatic zone at the bottom of the narrow Greenland transitional crust, and by indications for a 15° to 20° eastward dipping Moho from gravity data [*Speece*, 1992] and seismic data [*Larkin*, 1992] along the SW Greenland fjords. The available seismic data, however, are not sufficient to place more confidence in this suggestion. More deep seismic data are needed from the Greenland margin and, in particular, from the Labrador shelf.

CONCLUSIONS

An analysis of seismic data offers new insights into the deep crust underneath the shelf parallel to the passive margin of SW Greenland and provides new constraints on the magmatic rifting history of the northern Labrador Sea. Land stations along the coast recorded wide-angle reflection data from a marine air gun shot profile along the shelf. Due to dense shot spacing, we identified numerous upper, middle, and lower crustal seismic phases. Correlations of phases from near-vertical to postcritical offsets allowed us to derive a velocity/depth model for the crust. High-amplitude lower crustal and Moho reflections from the top and bottom of a high-velocity zone at the base of the crust have been identified. Tau-p analyses and 1-D inversion indicated a HVZ at the bottom of the crust with velocities larger than 7.2 km/s. Combined 2-D travel time forward modeling and inversion produced a velocity/depth model that contains midcrustal and lower crustal discontinuities between 12 and 25 km depth and a Moho at 30 to 42 km depth, dipping northward. An average crustal velocity of about 6.6 km/s indicates a high proportion of mafic components in the crust. The lowermost crust consists of an up to 8-km-thick HVZ of temperature-corrected velocities between 7.5 and 7.85 km/s, suggesting mafic to ultramafic composition. Recrystallization of mafic material may have occurred under garnet-granulite facies condition during emplacement in lower crustal depths.

Evidence for a high-velocity, underplated mafic to ultramafic zone at the base of the thinned continental or transitional crust suggests that magmatism was present during the rifting and initial divergence of the northern and central Archean block of Greenland and Labrador. Large amounts of mantle-derived material must have been added to the crust but did not penetrate it, as indicated by the lack of mafic extrusives in SW Greenland. The lack of a HVZ at the bottom of the transitional crust along the southern Archean block about 500 km south of our profile [*Chian and Louden*, 1992] indicates that mafic underplating did not continue farther south. It seems reasonable to associate the underplated layer with the presence of rift-related mafic extrusives farther north on Disko Island and surroundings. This thick underplated layer in our study area could, therefore, be related to a possible hot spot magmatism in the Davis Strait [*White and McKenzie*, 1989] that produced volcanics in the Davis Strait region and underplated mafics and ultramafics in the northern Labrador Sea.

The identification of continuous and distinct reflections from the lower crust and Moho is a result of the high air gun shot density (trace density). Without high-quality wide-angle reflection data, the tremendous amount of unexposed magmatism along the shelf of SW Greenland associated with rifting would have gone unrecognized.

Acknowledgments. The cooperation of Ingve Kristoffersen (University of Bergen), Victor McGregor (Greenland), Jim Fowler (IRIS), the National Survey and Cadastre of Denmark (former Geodetic Institute), and the Geological Survey of Greenland is gratefully appreciated. Peter Skjellerup assisted in the data processing. Special thanks to the members of the University of Wyoming seismic crew, Chris Humphreys, Reid Fletcher, Alan Tanner, Rick Blenkner, Mark Skelton, Marvin Speece, and to the crew of the RV *Håkon Mosby*. We are grateful to Colin Zelt, who provided the 2-D travel time inversion program and commented on this paper. Critical comments by David Fountain, Rob Hawman, Ramon Carbonell, Nick Boyd, Bill Clement, Steve Larkin, and Jim Chalmers are very much appreciated. Reviews by Tom Brocher, Deborah Hutchinson, and Keith Louden helped improve the manuscript. The project was supported by NSF grants DPP-8821974 and DPP-9023847.

REFERENCES

Austin, J. A., P. L. Stoffa, J. D. Phillips, J. Oh, D. S. Sawyer, G. M. Purdy, E. Reiter, and J. Makris, Crustal structure of the structure of the southeast Georgia embayment-Carolina trough: Preliminary results of a composite seismic image of a continental suture(?) and a volcanic passive margin, *Geology, 18*, 1023-1027, 1990.

BABEL Working Group, Recording marine airgun shots at offsets between 300 and 700 km, *Geophys. Res. Lett., 18*, 645-648, 1991.

Bessonova, E. N., V. M. Fishman, V. Z. Ryaboyi, and G. A. Sitnikova, The tau method for inversion of travel times, I, Deep seismic sounding data, *Geophys. J. R. Astron. Soc., 36*, 377-398, 1974.

Bridgwater, D., J. Watson, and B. F. Windley, The Archaean craton of the North Atlantic region, *Philos. Trans. R. Soc. London, Ser. A, 273*, 493-512, 1973.

Bridgwater, D., L. Keto, V. R. McGregor, and J. S. Myers, Archean gneiss complex of Greenland, in *Geology of Greenland*, edited by A. Escher and W. S. Watt, pp. 18-74, Grønlands Geologiske Undersøgelse, Copenhagen, 1976.

Brocher, T. M., and M. J. Moses, Wide-angle seismic recordings obtained during the TACT multichannel reflection profiling in the northern Gulf of Alaska, *U.S. Geol. Survey Open File Rep., 90-663*, 1990.

Burke, M. M., and D. M. Fountain, Seismic properties of rocks from an exposure of extended continental crust - new laboratory measurements from the Ivrea Zone, *Tectonophysics, 182*, 119-146, 1990.

Chalmers, J. A., New evidence on the structure of the Labrador Sea/Greenland continental margin, *J. Geol. Soc. London, 148*, 899-908, 1991.

Chian, D., and K. Louden, The structure of Archean-Ketilidian crust along the continental shelf of southwestern Greenland from a seismic refraction profile, *Can. J. Earth Sci., 29*, 301-313, 1992.

Christensen, N. I., and D. M. Fountain, Constitution of the lower continental crust based on experimental studies of seismic velocities in granulite, *Geol. Soc. Am. Bull., 86*, 227-236, 1975.

Clarke, D. B., Tertiary basalts of Baffin Bay: Possible primary magma from the mantle, *Contrib. Mineral. Petrol., 25*, 203, 1970.

Clarke, D. B., and A. K. Pederson, Tertiary volcanic province of west Greenland, in *Geology of Greenland*, edited by A. Escher and W. S. Watt, pp. 365-385, Geological Survey of Greenland, Copenhagen, 1976.

Clarke, D. B., and B. G. J. Upton, Tertiary basalts of Baffin Island: Field relations and tectonic setting, *Can. J. Earth Sci., 8*, 248-258, 1971.

Denham, L. R., Offshore geology of northern West Greenland (69 to 75° N), *Rep. Geol. Surv. Greenland, 63*, 1974.

Diebold, J. B., and P. L. Stoffa, The travel-time equation, tau-p mapping, and inversion of common midpoint data, *Geophysics, 46*, 238-254, 1981.

Fountain, D. M., The Ivrea-Verbano and Strona-Ceneri Zones, northern Italy: A cross-section of the continental crust–New evidence from seismic velocities, *Tectonophysics, 33*, 145-165, 1976.

Fountain, D. M., Growth and modification of lower continental crust in extended terrains: The role of extension and magmatic underplating, in *Properties and Processes of Earth's Lower Crust*, *Geophys. Monogr. Ser.*, vol. 51, edited by R. F. Mereu, S. Mueller, and D. M. Fountain, pp. 287-299, AGU, Washington, D.C., 1989.

Fountain, D. M., M. H. Salisbury, and J. Percival, Seismic structure of the continental crust based on rock velocity measurements from the Kapuskasing uplift, *J. Geophys. Res., 95*, 1167-1186, 1990.

Friend, C. R. L., and A. P. Nutman, Refolded nappes formed during late Archaean terrane assembly, Godthåbsfjord, southern West Greenland, *J. Geol. Soc. London, 148*, 507-519, 1991.

Furlong, K. P., and D. M. Fountain, Continental crustal underplating: thermal considerations and seismic-petrologic consequences, *J. Geophys. Res., 91*, 8285-8294, 1986.

Geological Survey of Canada, Gravity anomaly map of the continental margin of eastern Canada, *Map 1708A*, scale 1:500,000, Ottawa, Ont., 1988*a*.

Geological Survey of Canada, Magnetic anomaly map of the continental margin of Eastern Canada, *Map 1709A*, scale 1:500,000, Ottawa, Ont., 1988*b*.

Geological Survey of Greenland, Geological map of Greenland, sheet 2, Frederikshåb Isblink - Søndre Strømfjord, scale 1:500,000, Copenhagen, 1982.

GLIMPCE Seismic Refraction Working Group, GLIMPCE seismic experiments - long offset recordings, *EOS Trans. AGU, 70*, 841, 852-853, 1989.

Gohl, K., S. B. Smithson, and Y. Kristoffersen, The structure of the Archean crust in SW Greenland from seismic wide-angle data: A preliminary analysis, in *Continental Lithosphere: Deep Seismic Reflections*, *Geodyn. Ser.*, vol. 22, edited by R. Meissner, L. Brown, H.-J. Dürbaum, W. Franke, K. Fuchs, and F. Seifert, pp. 53-57, AGU, Washington, D.C., 1991.

Hawman, R. B., and R. A. Phinney, Analysis of sparse wide-angle reflection data in the tau-p domain, *Bull. Seismol. Soc. Am., 81*, 202-221, 1991.

Hinz, K., H.-U. Schlüter, A. C. Grant, S. P. Srivastava, D. Umpleby, and J. Woodside, Geophysical transects of the Labrador Sea: Labrador to southwest Greenland, *Tectonophysics, 59*, 151-183, 1979.

Hyndman, R. D., Evolution of the Labrador Sea, *Can. J. Earth Sci., 10*, 637-664, 1973.

Hyndman, R. D., Marginal basins of the Labrador Sea and the Davis Strait hot spot, *Can. J. Earth Sci., 12*, 1041-1045, 1975.

Johnson, G. L., S. P. Srivastava, J. Campsie, and M. Rasmussen, Volcanic rocks in the Labrador Sea and environs and their relationship to the evolution of the Labrador Sea, in Current Research, Part B, *Pap. Geol. Surv. Can. 82-1B*, 7-20, Geol. Surv. of Canada, 1982.

Keen, C. E., and B. de Voogt, The continent-ocean boundary at the rifted margin off eastern Canada: New results from deep seismic reflection studies, *Tectonics, 7*, 107-124, 1988.

Keen, M. S., and G. L. Williams (Eds.), *The Geology of North America*, vol. I-1, *Geology of the Continental Margin of Eastern Canada*, p. 8, Geological Survey of Canada, Ottawa, Ont., 1990.

Kennett, B. L. M., and J. A. Orcutt, A comparison of travel time inversions for marine refraction profiles, *J. Geophys. Res., 81*, 4061-4070, 1976.

Kern, H., and A. Richter, Temperature derivatives of compressional and shear wave velocities in crustal and mantle rocks at 6 kbar confining pressure, *J. Geophys., 49*, 47-56, 1981.

Larkin, S. P., Crustal structure of a rifted Archean block, Ameralik, South West Greenland, M.S. thesis, 101 pp., Univ. of Wyo., Laramie, 1992.

LASE Study Group, Deep structure of the US East Coast passive margin from large aperture seismic experiments (LASE), *Mar. Pet. Geol., 3*, 234-242, 1986.

Laughton, A. S., South Labrador Sea and the evolution of the North Atlantic, *Nature, 232*, 612-617, 1971.

Laughton, A. S., The southern Labrador Sea - A key to the Mesozoic and early Tertiary evolution of the North Atlantic, *Initial Rep. Deep Sea Drill. Proj., 12*, 1155-1179, 1972.

Le Pichon, X., R. D. Hyndman, and G. Pautot, Geophysical study of

the opening of the Labrador Sea, *J. Geophys. Res., 76*, 4724-4743, 1971.

Lister, G. S., M. A. Etheridge, and P. A. Symonds, Detachment faulting and the evolution of passive continental margins, *Geology, 14*, 246-250, 1986.

Lister, G. S., M. A. Etheridge, and P. A. Symonds, Detachment models for the formation of passive continental margins, *Tectonics, 10*, 1038-1064, 1991.

Manderscheid, G., The geology of the offshore sedimentary basin of West Greenland, in Facts and Principles of World Petroleum Occurrence, edited by A. D. Miall, *Mem. Can. Soc. Pet. Geol., 6*, 951-974, 1980.

McCarthy, J., and G. A. Thompson, Seismic imaging of extended crust with emphasis on the western United States, *Geol. Soc. Am. Bull., 100*, 1361-1374, 1988.

McGregor, V. R., A. P. Nutman, and C. R. L. Friend, The Archean geology of the Godthåbfjord region, southern West Greenland, *Tech. Rep. 86-04*, pp. 113-169, Lunar and Planet. Inst., Houston, Tex., 1986.

McKenzie, D., Some remarks on the development of sedimentary basins, *Earth Planet. Sci. Lett., 40*, 25-32, 1978.

McMechan, G. A., and R. Ottoloni, Direct observation of a p-tau curve in a slant stacked wave field, *Bull. Seismol. Soc. Am., 70*, 775-789, 1980.

Nutman, A. P., C. R. L. Friend, H. Baadsgaard, and V. R. McGregor, Evolution and assembly of Archean gneiss terranes in the Godthåbsfjord region, southern West Greenland: Structural, metamorphic, and isotopic evidence, *Tectonics, 8*, 573-589, 1989.

Phinney, R. A., K. Roy Chowdhury, and L. N. Frazer, Transformation and analysis of record sections, *J. Geophys. Res., 86*, 359-377, 1981.

Reid, I. D., and C. E. Keen, Deep crustal structure beneath a rifted basin: results from seismic refraction measurements across the Jeanne d'Arc Basin, offshore eastern Canada, *Can. J. Earth Sci., 27*, 1462-1471, 1990*a*.

Reid, I. D., and C. E. Keen, High seismic velocities associated with reflections from within the lower oceanic crust near the continental margin of eastern Canada, *Earth Planet. Sci. Lett., 99*, 118-126, 1990*b*.

Roest, W. R., and S. P. Srivastava, Sea-floor spreading in the Labrador Sea: A new reconstruction, *Geology, 17*, 1000-1003, 1989.

Speece, M. A., Geophysical studies in Precambrian regions: the Laramie Mountains, Wyoming, and the Godthåbsfjord area, southern West Greenland, Ph.D. dissertation, Univ. of Wyo., Laramie, 1992.

Srivastava, S. P., Evolution of the Labrador Sea and its bearing on the early evolution of the North Atlantic, *Geophys. J. R. Astron. Soc., 52*, 313-357, 1978.

Srivastava, S. P., Davis Strait: Structures, origin and evolution, in *Structure and Development of the Greenland-Scotland Ridge*, edited by M. H. P. Bott, S. Saxov, M. Talwani, and J. Thiede, pp. 159-189, Plenum, New York, 1983.

Srivastava, S. P., and C. R. Tapscott, Plate kinematics of the North Atlantic, in *The Geology of North America*, vol. M, *The Western North Atlantic Region*, edited by P. R. Vogt and B. E. Tucholke, Chapter 23, pp. 379-404, Geological Society of America, Boulder, Colo., 1986.

Srivastava, S. P., R. K. H. Falconer, B. MacLean, Labrador Sea, Davis Strait, Baffin Bay: Geology and geophysics–A review, *Mem. Can. Soc. Pet. Geol., 7*, 333-398, 1980.

Stergiopoulos, A. B., Geophysical crustal studies off the southwest Greenland margin, M.S. thesis, Dalhousie Univ., Halifax, Nova Scotia, 1984.

Stoffa, P. L., P. Buhl, J. B. Diebold, and F. Wenzel, Direct mapping of seismic data to the domain of intercept time and ray parameter: A plane wave decomposition, *Geophysics, 46*, 255-267, 1981.

Taylor, F. C., The Nain Province, in Variations in Tectonic Styles in Canada, edited by R. A. Price and R. J. W. Douglas, *Spec. Pap. 11, Geol. Assoc. Can.*, 435-452, 1972.

Thorning, L., Aeromagnetic maps of parts of southern and central West Greenland, *Rapp. 122*, Grønlands Geol. Undersøl., Copenhagen, 1984.

Thorning, L., A decade of geophysical surveying in Greenland, in Developments in Greenland Geology, edited by F. Kalsbeek and W. S. Watt, *Rapp. 128*, pp. 12-133, Grønlands Geol. Undersøl., Copenhagen, 1986.

Tréhu, A. M., A. Ballard, L. M. Dorman, J. F. Gettrust, K. D. Klitgord, and A. Schreiner, Structure of the lower crust beneath the Carolina Trough, U.S. Atlantic continental margin, *J. Geophys. Res., 94*, 10,585-10,600, 1989.

van der Linden, W. J. M., Crustal attenuation and sea floor spreading in the Labrador Sea, *Earth Planet. Sci. Lett., 27*, 409-423, 1975.

Weigel, W., G. Wissmann, and P. Goldflam, Deep seismic structure (Mauritania and Central Morocco), in *Geology of the Northwest African Continental Margin*, edited by U. van Rad, K. Hinz, M. Sarntheim, and E. Seibold, pp. 132-159, Springer-Verlag, New York, 1982.

White, R., and D. McKenzie, Magmatism at rift zones: The generation of volcanic continental margins and flood basalts, *J. Geophys. Res., 94*, 7685-7729, 1989.

Woodside, J. M., and J. Verhoef, Geological and tectonic framework of eastern Canada as interpreted from potential field imagery, *Pap. Geol. Surv. Can., 88-26*, 1989.

Zelt, C. A., and R. M. Ellis, Practical and efficient ray tracing in two-dimensional media for rapid traveltime and amplitude forward modelling, *Can. J. Explor. Geophys., 24*, 16-31, 1988.

Zelt, C. A., and R. B. Smith, Seismic traveltime inversion for 2-D crustal velocity structure, *Geophys. J. Int., 108*, 16-34, 1992.

K. Gohl, Alfred Wegener Institute for Polar and Marine Research, Postfach 120161, D-2850 Bremerhaven, Germany.

S.B. Smithson, Department of Geology and Geophysics, University of Wyoming, Laramie, WY 82071-3006.

(Received November 12, 1991;
revised December 14, 1992;
accepted December 29, 1992.)